Intercalation of Bi nanoparticles into graphite enables ultra-fast and ultra-stable anode material for Sodium-ion batteries

Journal:	*Energy & Environmental Science*
Manuscript ID	EE-COM-10-2017-003016.R1
Article Type:	Communication
Date Submitted by the Author:	26-Jan-2018

Complete List of Authors:	Chen, Ji; University of Maryland at College Park, Chemical & Biomolecular Engineering Fan, Xiulin; University of Maryland, Department of Chemical & Biomolecular Engineering Ji, Xiao; University of Maryland, Department of Chemical & Biomolecular Engineering Gao, Tao; University of Maryland at College Park Hou, Singyuk; University of Maryland, Department of Chemical & Biomolecular Engineering Zhou, Xiuquan; University of Maryland, Department of Chemistry and Biochemistry Wang, Luning; University of Maryland, Department of Chemistry and Biochemistry Wang, Fei; University of Maryland at College Park, ; University of Maryland Yang, Chongyin; University of Maryland at College Park, Chen, Long; University of Maryland, Department of Chemical & Biomolecular Engineering Wang, Chunsheng; University of Maryland, Department of Chemical & Biomolecular Engineering

Energy & Environmental Science

Cite this: DOI: 10.1039/c0xx00000x

www.rsc.org/xxxxxx

Communication

Intercalation of Bi nanoparticles into graphite enables ultra-fast and ultra-stable anode material for Sodium-ion batteries

Ji Chen,[†,1] Xiulin Fan,[†,1] Xiao Ji,[1] Tao Gao,[1] Singyuk Hou,[1] Xiuquan Zhou,[2] Luning Wang,[2] Fei Wang,[1] Chongyin Yang,[1] Long Chen,[1] and Chunsheng Wang*[,1]

Received (in XXX, XXX) Xth XXXXXXXXX 20XX, Accepted Xth XXXXXXXXX 20XX
DOI: 10.1039/b000000x

Sodium ion batteries (SIBs) have been revived as important alternative energy storage devices for the large-scale energy storage, which requires SIBs to have long cycling life and high power density. However, scarcity of suitable anode materials hinders the application. Herein, we report a Bismuth intercalated graphite (Bi@Graphite) anode material, which is substantially different from the previously reported metal@Graphene. In Bi@Graphite, Bi nanoparticles between graphite interlayers enhance the capacity, while graphite sheath provides a robust fast electronic connection for long cycle stability. The Bi@Graphite possesses a safe average storage potential of approximately 0.5 V vs. Na/Na^+, delivers a capacity of ~160 mAh g^{-1} at 1C (160 mA g^{-1}), exhibits outstanding cycling stability (ca. 90% capacity retention for 10000 cycles at 20C), and can maintain 70% capacity at 300C (~ 110 mAh g^{-1} at 48 A g^{-1}), which is equivalent to full charge/discharge in 12 s. Bi@Graphite demonstrates the highest rate-capability ever reported among all anodes for SIBs. Detailed characterization results indicate that unique Bi nanoparticle-in-graphite structure and fast kinetics of ether co-intercalation into graphite are responsible for these significant improvements that could translate into SIBs with excellent power densities.

Introduction

The past decades have witnessed the rapid development of renewable energy sources, such as the wind, the tide, and the solar energy. However, these energy sources are not continuously available. Large-scale electric energy storage battery system is becoming extremely important to realize the smooth integration of these intermittent energies into the grid because of its flexibility, high energy conversion efficiency and simple maintenance.[1] Sodium-ion batteries (SIBs) have aroused a great deal of interest recently, particularly for large scale stationary energy storage applications, due to the practically abundant and environmentally benign sodium.[2] The major criteria of stationary batteries for energy storage systems are long cycle life, high rate capability, low cost, and high safety. Hence, an abundant, nontoxic, stable, and high-rate electrode material for SIBs needs to be developed to ensure large-scale and long-term applications, and to decrease battery management cost.

Broader Context

Sodium-ion batteries (SIBs) have aroused a great deal of interest recently, particularly for large scale stationary energy storage applications, due to the practically abundant and environmentally benign sodium. The major criteria of stationary batteries for energy storage systems are long cycle life, high rate capability, low cost, and high safety. Exploration of high-rate anodes with long cycling life is urgently needed. Herein, for the first time, we reported the fabrication of Bismuth intercalated graphite (Bi@Graphite) material through intercalation-conversion reactions. The as-prepared material exhibits the highest capacity retention at high rate (70% at 300C, equivalent to full charge/discharge in 12 s) and one of the longest cycle stability (ca. 90% capacity retention for 10000 cycles at 20C) in all reported anodes for SIBs. The exceptional rate capability and cycling stability of Bi@Graphite is attributed to the unique sandwich structure with Bi nanoparticles uniformly distributed among the conductive protecting graphite sheath. The Metal@Graphite with metal nanoparticles intercalated in graphite layers offers a new direction for exploration of next generation of electrode materials for rechargeable batteries.

Extensive researches have been devoted to develop long cycling and high power density electrode materials. Significant performance advances have been achieved in cathodes. Cathode materials with NASICON,[3, 4] P2,[5, 6] or O3,[7] structures exhibited long cycling stability as well as high rate capability. However, the advance in anode materials in terms of high rate capability and long cycling stability is still unsatisfactory. Intercalation anodes, for example the well-known LiC_6 in Li-ion batteries (LIBs), which belongs to binary graphite intercalation compounds (GIC), cannot be formed as effectively in SIBs, because of the crystalline mismatch between graphite lattice and sodium ions.[8] Until recently, Philipp et al. has solved the unfavorable mismatch issue through the mechanism of sodium co-intercalation with ether solvents, forming ternary GICs.[9] They demonstrated the stable cycling of 1,000 cycles. Unfortunately, the low capacity of ~110 mAh g^{-1} and density (~2.25 g cm^{-3}) cause low gravimetrical and volumetric energy densities. More recently, Kang et al[10] further revealed the excellent rate performance (50% capacity retention achieved at a high current density of 10 A g^{-1} with respect to capacity at a low current density of 1 A g^{-1}) of natural graphite in ether electrolytes, making graphite an ideal platform for developing high-rate anodes for SIBs. Unlike graphite, hard carbon can deliver higher capacity,[11] however the

rate capability and cycle life are still not satisfactory.[12] Moreover, the low sodium intercalation potential of hard carbon facilitates the detrimental sodium dendrite formation, especially at high rates, making hard carbon unsuitable as the anode materials for large-scale energy storage batteries. On the other hand, theoretical calculation suggests that group IVA and VA metals such as Sn, Sb, Bi, are capable of delivering high capacities by forming Na-rich alloys.[13] Despite of the high theoretical capacity, the practical application of these alloy-based anode materials for SIBs is still a huge challenge. One commonly recognized reason is the capacity decay caused by aggregation (slower kinetics due to loss of nanoscale diffusion distance) and pulverization (loss of electrical contact) of active materials, which is induced by severe volume variation during sodiation/desodiatioin. The strategies toward improving the cycle life of alloy-type anodes mainly focus on designing efficient nanostructures and introducing conductive carbon host/substrate (e.g., carbon nanofibers, graphene), but only limited improvement in the reaction kinetics and cycle life has been achieved.[14] Among the applied conductive carbon matrices, graphene has emerged as an attractive alternative to other carbon allotropes because of its fascinating electronic, thermal, and mechanical properties, high specific surface areas, and easy availability from graphite.[15] However, these methods usually consist of tedious oxidation-exfoliation of graphite, anchoring of metal precursor onto graphene oxide (GO) and reducing of GO and metal precursor to get reduced graphene oxide (rGO) and metal particles, respectively.[16] The obvious drawback of these strategies is that the procedure inevitably increases the environmental imperilment, augments the preparation cost, and adds complexity to the preparation processes.[17] On the other hand, in such formed composites, graphene is loosely stacked with a much lower conductivity compared with the graphite because of plenty of defects on the basal plane. The large surface metal/rGO normally leads to large irreversible capacity.[13] Moreover, large volume change of metal alloy upon sodium ion insertion can only be accommodated to a limited degree, which offers only a modest improvement in cycling stability. It is highly desirable to take advantage of the above excellent properties of graphene while maintaining the close contact between metal and graphene as well as the integrity of graphene and graphite structure.

Herein, for the first time we report a method of direct intercalation of metal nanoparticles (NPs) into graphite layers through the GIC route (Figure 1). Bi was chosen as a model metal to demonstrate this idea because of its high theoretical gravimetric capacity of 385 mAh g^{-1}, extremely high volumetric capacity (3765 mAh cm^{-3}) and favorable sodium alloy potential (0.5 V vs. Na^+/Na) to avoid dendrite formation. Novel sandwich-like Bi@Graphite was synthesized via an intercalation-transformation method. Details for the synthesis and mechanism are included in the supplementary information. In such a system, Bi NPs are intercalated between the adjacent graphene layers and tightly immobilized, which can provide a buffer matrix for the volume change of Bi during the charge-discharge cycling, and effectively maintains the active surface and leaves stable and open channels for ion transport. Meanwhile, the low-defect graphene layers in graphite provide higher electrical conductivity and structural scaffold to prevent the aggregation of Bi, enabling the Bi@Graphite extremely fast charge-discharge capacity (70% capacity retention at 300C with respect to 1C) as well as excellent stability (90% capacity retention for over 10000 cycles). Detailed characterizations show that the unique layered structure with Bi nanoparticles confined among the graphite layers plays the key role in the long cycling stability and the ultra-fast rate capability.

Results and Discussion

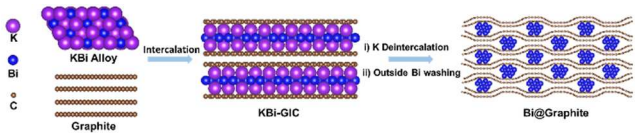

Fig. 1 Schematic illustration for the synthesis of Bi@Graphite.

Overall strategy for synthesis of Bi@Graphite is schematically depicted in Figure 1. A detailed description is given in the experimental section. Briefly, KBi alloy was first synthesized by heating the mixture of K and Bi in a double quartz ampule at 550 ^oC. X-ray diffraction (XRD) data of heated K & Bi mixture (Figure S1a) indicate successful alloying of K and Bi, which is also supported by the greenish color of alloy (K_3Bi) after synthesis. Subsequently, the KBi alloy was mixed with highly crystalized graphite (Figure S1b) and Bi by hand milling using mortar and pestle in a glove box, and then sealed under vacuum in a double ampule setup again and heated to 550 ^oC for intercalation. The XRD pattern of the as-synthesized KBi-GIC powders showed several peaks with d-spacings of 13.26, 6.62, and 4.42 Å (Figure 2a), corresponding to the reflections of (001), (002), and (003), respectively. This suggests a stage-IIα-type structure, where KBi alloy intercalates in between every two graphene layers ($KBi_{0.6}C_8$). The absence of the (002) reflection at 2θ=26.6^o of graphite suggests a complete intercalation of graphite by the KBi adducts. The stoichiometry of this stage-IIα KBi-GIC is $KBi_{0.6}C_8$ as previously determined by chemical analysis.[18] For the next step, the as-prepared KBi-GIC was initially washed with ethanol to deintercalate K in KBi-GIC to form Bi@GIC,[19] and also to react with unintercalated KBi alloy yielding Bi, which was evidenced by the emergence of strong Bi reflections in the XRD pattern (Bi+Bi@Graphite in Figure 2a). These strong Bi reflections are from two different groups of Bi particles (Bi outside & Bi@Graphite). The Bi metal particles outside the graphite is then removed by washing with dilute nitric acid, while the Bi intercalated between graphite sheets in Bi@Graphite were well-protected by the graphite layers from nitric acid, as demonstrated by Bi diffraction peaks in XRD pattern of Bi@Graphite in the Figure 2a. The inside Bi NPs are well protected by micro-sized graphite substrate with low surface area, which are expected to achieve higher reversible capacity, better rate performance, and long cycle life.

The XRD peaks of Bi in Bi@Graphite is much broader compared to Bi peaks in the XRD patterns of Bi+Bi@Graphite or Bi. The broadening of these peaks suggested significant reducing in crystallite sizes of Bi after intercalation-deintercalation, and the crystallite sizes were estimated from XRD data using the broadening analysis proposed by Balzar et al.[20] and implemented in the TOPAS 4.2 package.[21] LaB_6 standard was used for the calibration of instrument broadening, and the subsequent refinement procedures were described elsewhere.[22] The

broadening analysis gave crystallite sizes of 11±1, 46±3, and 193±10 nm for the Bi phase in Bi@Graphite, Bi+Bi@Graphite, and Bi samples, respectively (Figure S2). This is expected for

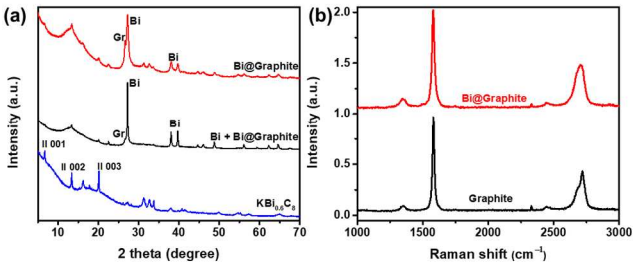

Fig. 2 (a) XRD patterns for the as-synthesized $KBi_{0.6}C_8$, Bi+Bi@Graphite, and Bi@Graphite; (b) Raman spectra of graphite and Bi@Graphite.

Bi@Graphite since all of the Bi nanoparticles are located between the graphite layers. During the deintercalation of K, the graphite layers blocked the possible aggregation of the Bi NPs, resulting in a much smaller crystallite size for Bi in Bi@Graphite.

The graphite structure in Bi@Graphite is characterized using Raman spectroscopy, which is a powerful tool for studying the structure of graphitic carbon materials. Usually, the Raman spectrum of graphitic carbon material consists of the D-, G-, and 2D-bands of carbon. The D-band (1330−1340 cm^{-1}) is associated with the defect-activated breathing modes of six-membered carbon rings, and the G-band (1580−1600 cm^{-1}) is assigned to the E_{2g} phonons at the Brillouin zone center, while the 2D band corresponds to the second order of zone-boundary phonons.[23, 24] Specifically, the intensity ratio of D- to G-bands, I_D/I_G, reflects the defect density in graphene.[25, 26] It should be noted that our method is non-destructive to graphene sheets, as confirmed by the negligible increase of I_D/I_G from 0.072 for graphite to 0.094 for Bi@Graphite, which is in sharp contrast to the common value of 0.8-1.7 for GO and rGO.[27] The major difference between the Raman spectra of graphite and Bi@Graphite is the 2D feature. The 2D peak in bulk graphite consists of two components 2D1 and 2D2, typical for graphite or >5 layer graphene. While the 2D peak for Bi@Graphite is much broader with respect to graphite, indicating the existence of few-layer graphene in Bi@Graphite.[24] Usually, after deintercalation of intercalatants, the graphite structure can be fully restored by restacking of graphene sheets. The unusual phenomenon in the case of Bi@Graphite reflects that the remaining Bi NPs act as spacers located in between graphene sheets that prevent the full re-stacking of the graphene sheets.

The structure and the morphology of the Bi@Graphite were further characterized by scanning electron microscopy (SEM) and transmission electron microscopy (TEM) analysis. SEM images of the Bi@Graphite show a typical platelet structure (Figure 3a), similar to the precursor graphite (Figure S3), indicating that the flake morphology of the graphite has been well retained. Both the graphite and Bi@Graphite exhibit very smooth and clean surface (Figure S4), no Bi particles outside graphite can be observed in Bi@Graphite (Figure S4a). Instead, some particles can be seen under the superficial graphene sheets in the enlarged SEM images of Bi@Graphite. The existence of Bi in Bi@Graphite is further verified by elemental mapping using energy-dispersive X-ray spectroscopy (EDS). As shown in Figure 3b, the signal of Bi coincides with carbon signal from graphite except the carbon tape (for SEM testing) in the top right corner. Low-magnification SEM image and EDS mapping further confirmed the uniform Bi distribution in all of the graphite particles on a large scale (Figure

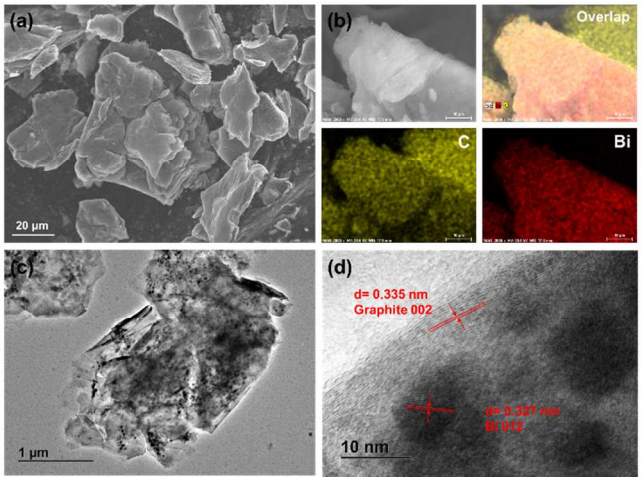

Fig. 3 (a) SEM image of the as-synthesized Bi@Graphite flakes; (b) SEM image and corresponding C, Bi, and overlapped elemental mapping images of Bi@Graphite; The carbon signals outside the particles are from the carbon tape. (c) TEM and (d) HRTEM image of the Bi@Graphite.

S5). Since no Bi NPs can be seen on the surface of Bi@Graphite, the Bi signal can only be attributed from the Bi inside graphite. The unique Bi-in-graphite structure in Bi@Graphite has been further proved by TEM. It can be clearly seen that the dark spots, which are Bi NPs, locate between the graphene layers in graphite (Figure 3c). The high-resolution TEM (HRTEM) image (Figure 3d) of the Bi@Graphite reveals two sets of lattice fringes: a spacing of 0.327 nm in NPs corresponding to the (012) planes of Bi; and 0.335 nm for graphite (002) planes at periphery, respectively.

As expected, Bi NPs is well preserved in Bi@Graphite, and tightly wrapped by graphene sheets in graphite as schematically demonstrated in Figure 1. It is the first report for synthesis of the metal nanoparticle intercalated graphite composite for metal ion batteries. The electrochemical performance of the Bi@Graphite as an anode material for SIBs was firstly evaluated using galvanostatic charge/discharge cycling. The specific capacity (mAh g^{-1}) and the current density (mA g^{-1}) are calculated based on the total mass of active material including both the Bi and graphite material. Figure 4a shows the charge-discharge curves of Bi@Graphite at 80 mA g^{-1} within the potential window of 1.8-0.01 V. The Bi@Graphite delivered a discharge capacity of ~220 mAh g^{-1} and a charge capacity of 164 mAh g^{-1} in the first cycle, corresponding to an initial Coulombic efficiency of 74.5%. The small amount of irreversible capacity is mainly attributed to reduction of surface functional groups of graphite with minor contribution from forming isolated solid electrolyte interface (SEI). This initial Coulombic efficiency is higher than those of graphene based anodes, which typically give values below 50%.[28] The overlap of subsequent discharge/charge curves indicates the excellent reversibility for the Bi@Graphite electrode during sodiation/desodiation cycles. It should be noted that the capacity of Bi@Graphite is 45% more than that of precursor graphite of~110 mAh g^{-1} (Figure S6a), indicating higher energy

density than that of graphite can be achieved using the Bi@Graphite electrodes. The capacity originated from graphite and Bi was calculated from the galvanostatic charge/discharge curves in Figure 4a by attributing the two 1:2 plateau capacity to Bi, which correspond to the two-step alloying reaction of Bi as expressed below:[29]

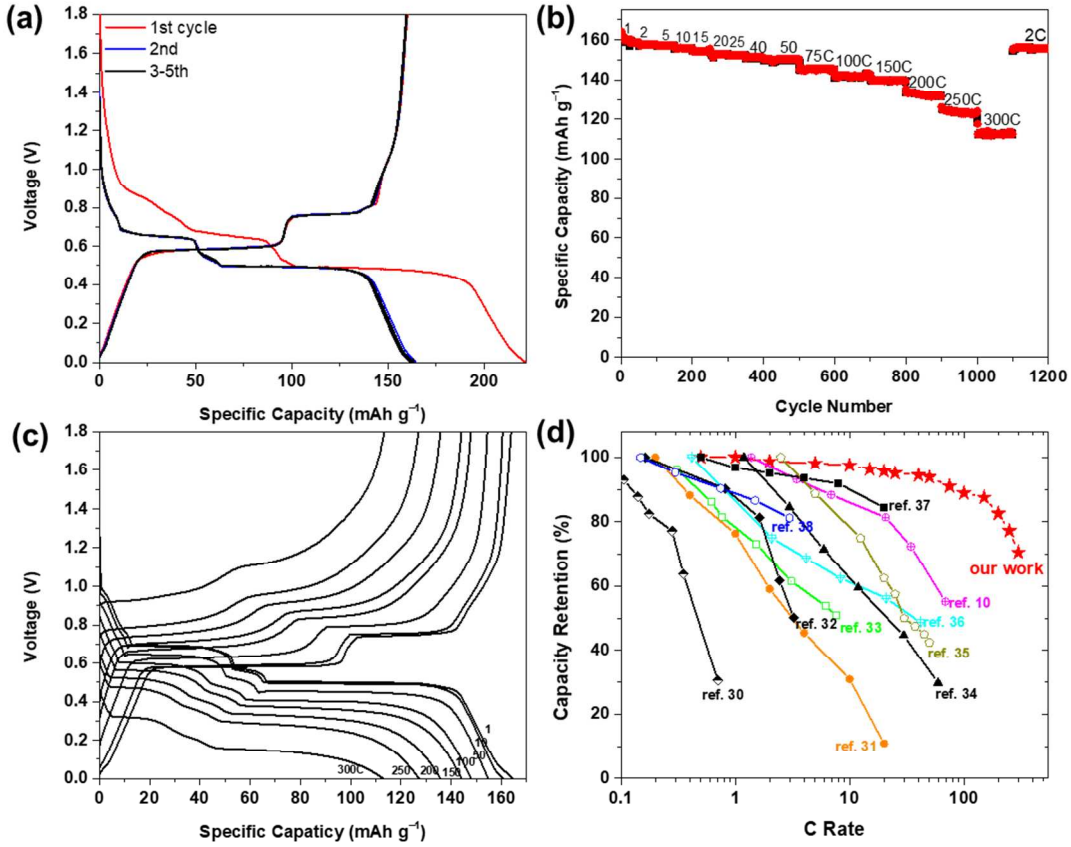

Fig. 4 (a) Galvanostatic charge/discharge curves of as-synthesized Bi@Graphite composite at a constant current of 80 mA g^{-1} in the voltage window 0.01-1.8 V at room temperature (25 °C); (b) rate capability at different charge/discharge rates; (c) voltage-capacity curves at different rates (increased from 1C to 300C); (d) Comparison of rate capability with reported anodes for SIBs.[10, 30-38]

$$Bi + Na^+ + e^- \leftrightarrow NaBi \quad (1)$$

$$NaBi + 2Na^+ + 2e^- \leftrightarrow Na_3Bi \quad (2)$$

Accordingly, graphite and Bi contributes to 54 and 106 mAh $g_{composite}^{-1}$, respectively. Given the 30% Bi content in Bi@Graphite determined by inductively coupled plasma-atomic emission spectroscopy (ICP-AES), the specific capacity with respect to Bi is 353 mAh g^{-1}, slightly higher than the capacity of pure Bi (~330 mAh g^{-1}) with micro-size after activation cycles (Figure S7a), indicating better utilization of Bi in the case of Bi@Graphite electrodes. On the other hand, the specific capacity of graphite is only 77 mAh g^{-1}, lower than the 110 mAh g^{-1} obtained from graphite electrodes (Figure S6a). The partial loss of capacity for the graphite is due to Bi NPs occupying spacesand spots where solvated sodium should be stored. It is also worth noting that the volumetric capacity was significantly increased by 88% from ~250 mAh cm^{-3} (co-intercalation capacity of graphite) to 470 mAh cm^{-3} for Bi@Graphite, which is beneficial for volumetric capacity-sensitive applications such as portable electronics and electrical vehicles.[39]

The unique Bi-in-graphite structure in Bi@Graphite enables its capability to be discharged/charged at ultra-high rates. A rate of nC corresponds to a full charge/discharge in 1/nh (according to the stable capacity of 160 mAh g^{-1} of Bi@Graphite, the rate of 1C indicates a discharge/charge current density of 160 mA g^{-1}). Figure 4b presents the rate capability of the Bi@Graphite composite with the corresponding charge-discharge curves plotted in Figure 4c. As can be observed, the Bi@Graphite electrode delivers a capacity of 155 mAh g^{-1} at 10C. At 100C discharge/charge rate (36 s to total charge or discharge), more than 140 mAh g^{-1} can still be achieved. Even at a much higher rate of 300C (12 s to full charge or discharge), a capacity of 113 mAh g^{-1} (70% of the capacity at 1C) is obtained. Moreover, when the rate is finally returned to 2C after over 1000 cycles, a capacity of 156 mA h g^{-1} (98.7 % of the initial 158 mA h g^{-1}) is recovered, implying the excellent tolerance for the rapid sodium ion insertion/extraction reactions as well as good stability of the Bi@Graphite electrode. To the best of our knowledge, the capacity retention of Bi@Graphite at high rates is the highest ever reported for anodes in SIBs (Figure 4d). In comparison, the Bi electrode can only retain 15.2% of its capacity when charged/discharged at 64C (Figure S7b-c). The clear difference in capacity retention at high rates demonstrates that the high rate capability of Bi@Graphite is closely related with its unique Bi-in-graphite structure.

To understand the mechanism for high rate capability of Bi@Graphite, the rate performance of graphite and microsized

pure Bi were also evaluated in the same electrolytes. As shown in Figure S6b, at a high rate of 300C, the graphite electrode can retain 80 mAh g^{-1} (74.8% with respect to 107 mAh g^{-1} at 1C). The charge/discharge curves of graphite electrode at different rates are shown in Figure S6c, demonstrating the fast kinetic of the graphite. This results are in accordance with previous reports on fast co-intercalation of graphite by ether-solvated sodium ions.[10] It is

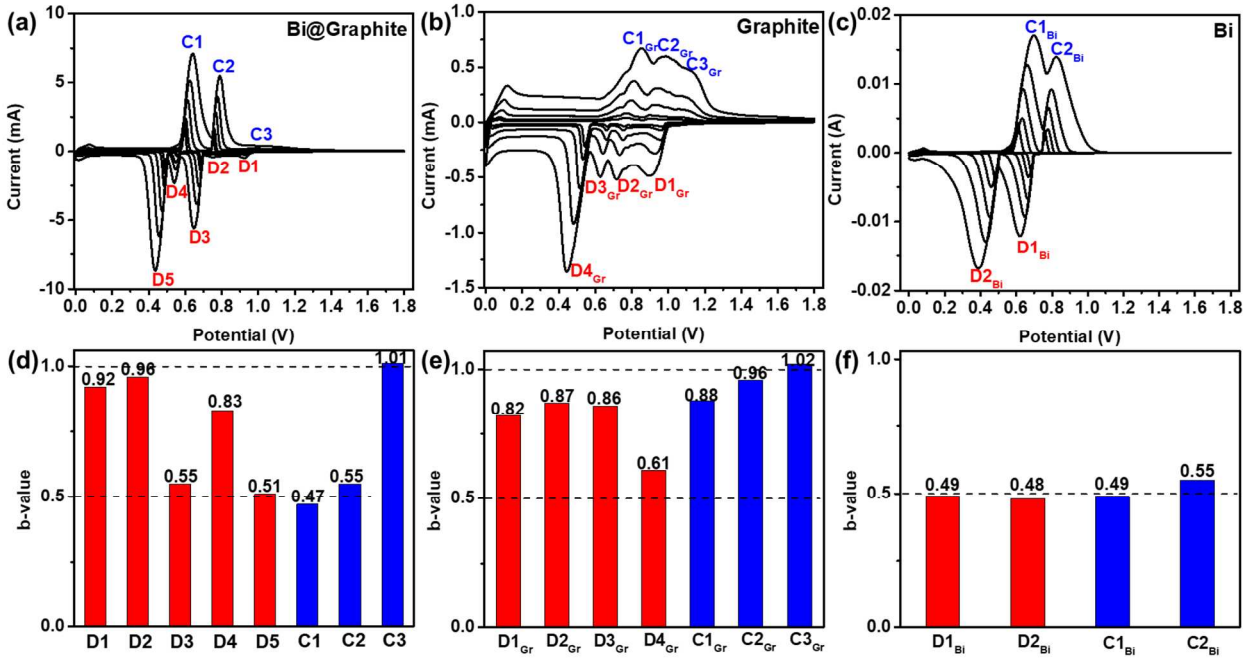

Fig. 5 (a-c) CV curves at different sweep rates (0.1-2 mV s^{-1}) of the (a) Bi@Graphite composite, (b) graphite, and (c) Bi electrode; (d-f) corresponding *b*-value of different current peaks

worth noting that the fast kinetics of co-intercalation into graphite can be clarified as follows. In the traditional carbonate electrolyte, SEI will be formed in the first discharge. The Li-ion intercalation into graphite have to disassociate the coordinated solvent first, and then transport through SEI, transfer the charge, and finally intercalate into graphite. The desolvation of Li-ion limits the reaction kinetics of electrochemical Li intercalation.[40] Different from the Li-ion intercalation, the co-intercalation of Na-ion with ether solvent (in our case, Na-ion with DME molecules) eliminates the desolvation step, which greatly accelerates the reaction kinetics. On the other hand, Bi anodes show much higher capacity (theoretical 385 mAh g^{-1}) but much worse rate capability (Figure S7b) than graphite (Figure S6b). To increase the graphite capacity without sacrificing the high rate performance, nano-sized Bi should be intercalated into graphite layer as we synthesized in Bi@Graphite, which also prevents the Bi pulverization/aggregation and maintains similar cycle life as the graphite. In addition, the uniform nanoscale (~ 10 nm) active material Bi affords a shorter Na^+ and electron transport pathway, enhancing alloying reaction kinetics and utilization of the active material upon discharge and charge. The Bi-in-graphite structure not only provides the excellent structural stability of the composite, but also provides continuous conductive paths between Bi NPs, and therefore reduces the particle to particle interfacial resistance.

The controlling step for the rate performance of the Bi@Graphite electrode was further investigated using cyclic voltammetry (CV) at different scan rates from 0.1 to 2 mVs^{-1} (Figure 5a). In theory, the voltammetric response of an electrode-active material at various sweep rates can be summarized as follows: [41]

$$i=av^b$$

in which the measured current (i) at a fixed potential obeys a power-law relationship with the potential sweep rate (v). For a redox reaction limited by semi-infinite diffusion, the peak current i follows a linear relationship with $v^{0.5}$ (i.e., b = 0.5); for a capacitive process, it varies with v (i.e., b=1).

As shown in Figure 5a, there are 5 distinguishable cathodic (discharge, sodiation) and 3 anodic (charge, desodiation) peaks in the CV curves of Bi@Graphite, denoted as D1-D5 (discharge) and C1-C3 (charge), respectively. The two largest peaks in the CV curves are in good agreement with the two main plateaus in discharge/charge curves. By careful comparing the CV curves of Bi@Graphite (Figure 5a), graphite (Figure 5b), and Bi (Figure 5c), we can assign peaks D1, D2, D4 in Bi@Graphite to graphite, and D3, D5 mainly to Bi, respectively. While the peaks C1, C2 are the overlapping of graphite and Bi capacity, C3 can be attributed solely to graphite. Figure 5d-f shows the b-value for each peak derived from linear fit of log(i) vs log(v) plots at every peak potential (Figure S8-10). It can be seen that graphite-related processes have b-values approaching 1, indicating a fast capacitive-dominant characteristic; while the Bi-related processes have b-values close to 0.5, indicating a redox reaction (alloying for the case of Bi) behavior.[29] Thus the whole capacity of Bi@Graphite can be divided into two parts, fast capacitive

capacity from graphite sheath and diffusion-controlled alloying

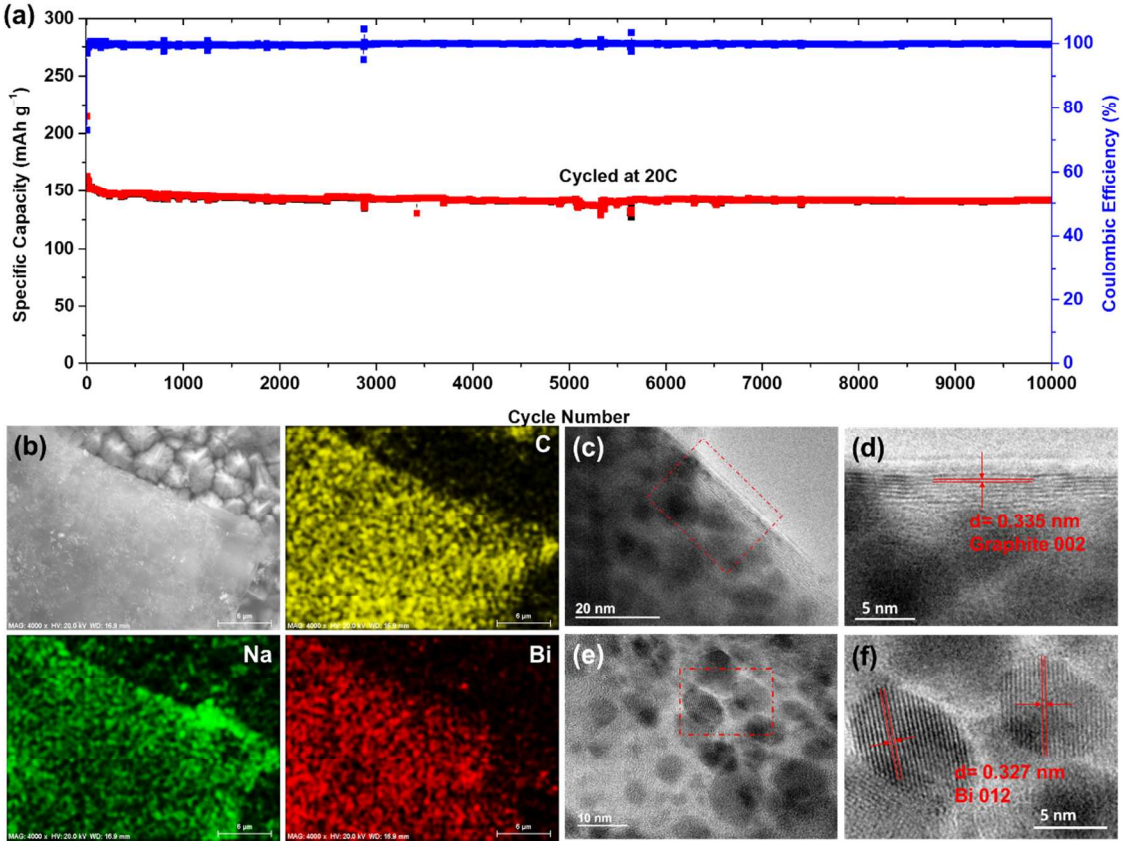

Fig. 6 (a) Cycling test at 20C after 20 cycles at 0.5C. (b) SEM image of the Bi@Graphite flakes on Cu foil after cycling and corresponding C, Na, and Bi, elemental mapping images; (c,e) TEM and (d,f) HRTEM images of the Bi@Graphite after cycling.

capacity from Bi cores.

Since all the rate performances for Bi@Graphite, graphite and Bi were tested in two-electrode Bi@Graphite||Na cell, the impact of Na counter electrode on the voltage polarization of the cells were evaluated in symmetry Na||Na cell using the same electrolyte. As shown in Figure S11a, the overpotential can be as high as ~300 mV when the current density reaches 30 mA cm^{-2} (corresponding to 300 C in Bi@Graphite||Na cell). Considering the symmetric Na||Na cell structure, it is believed that ~150 mV out of the overall ~350 mV overpotential (Figure 4c) in Bi@Graphite||Na is from the electrolyte and Na metal side at 300C (similar current density as shown in Figure S11b). Therefore, the rate performance will be further improved if an electrolyte with higher conductivity is employed and/or ultra-high rate cathode is paired.

The rate performance of the Bi@Graphite has also been tested at different temperatures from −20 to 60 °C (Figure S12). It is noted that this material can work well within the wide temperature range. At low temperatures, the rate capability becomes lower due to the decreased ionic conductivity of the electrolyte as well as more sluggish ion diffusion inside graphite. At high temperatures, the rate performance is slightly better than that at room temperature (25 °C) because of the increased ionic conductivity. By comparing the performance in the range of −20 to 60 °C, it can be concluded that at temperatures over 20 °C, the rate determination step is no longer the electrolyte conductivity but the ion transport inside the material. Another interesting phenomenon is the voltage shift of the graphite intercalation plateau. Graphite intercalation reaction is known to be exothermal, thus the lower the temperature, the more favourable the intercalation reaction, and the higher the intercalation potential. In our case, the voltage plateau of graphite intercalation reaction at 20 °C locates between the two plateaus of Bi sodiation. Upon heating to 60 °C, it downshifted and merged with the lower Bi sodiation plateau. When cooled down below 0 °C, it upshifted and merged with the higher Bi sodiation plateau. This further confirms the prior assignation of the 0.57 V plateau to co-intercalation of solvated Na^+ into graphite.

The Bi@Graphite electrode also shows exceptional cycling stability, as shown in Figure 6a and S13, the capacity retention is as high as ~90% for over 10,000 cycles at 20C and ~96% for over 600 cycles at 2C, respectively. It should be pointed out that the stable cycling is still on going without any decaying trend, and the cycling Coulombic efficiency is over 99.9%, higher than the typical values of ~98-99.5% for graphene-based materials.[28] The safe average discharge voltage of approximately 0.5 V, outstanding rate capability, and excellent cycling stability makes Bi@Graphite promising anode material for next-generation of

high energy low cost SIBs.

The morphology and the composition of the Bi@Graphite after cycling were characterized using SEM, TEM, and HRTEM techniques. Figure 6b shows the morphology and elemental mapping of Bi@Graphite after the 100th charge/discharge cycle. The original morphology of flake-like shape is well preserved. Moreover, the surface is smooth without any cracks (Figure S14), demonstrating the graphite is robust enough to accommodate the volume change of Bi NPs. As can be seen from the elemental mapping, the Bi element signal still overlaps the carbon element signal, similar to the elemental mapping results before cycling (Figure S15), indicating that Bi is still located among graphite layers after cycling. The detailed TEM and HRTEM images in Figure 6c-f also confirms that the Bi@Graphite core-sheath structure is retained. Bi NPs core indicated by lattice fringes of Bi 012 planes (Figure 6f) are well covered by graphite sheath indicated by graphite 002 planes (Figure 6d). This structure characteristic effectively provides a highly conductive pathway and highly stable matrix for the inner Bi NPs.

Conclusions

In summary, uniform Bi NPs with size of ~10 nm were successfully intercalated into the graphite layers by co-intercalation of K and Bi and then depotassiation. Benefiting from the unique sandwich structure with Bi NPs uniformly distributed among the graphite layers in conductive protecting graphite sheath, Bi@Graphite composites provide an extremely high rate capability (70% capacity retention at 300C with respect to 1C) at room temperature, which is the highest capacity retention for anode material for SIBs charge/discharged at such rate (Figure 4d). Besides, Bi@Graphite composite electrode can maintain a reversible capacity of 142 mAh g^{-1} at 20C after over 10,000 cycles with capacity retention of ~90%. Considering the low cost of the raw materials, the Bi@Graphite is an ideal anode material for stationary SIBs. On the other hand, the reported method provides a new way to synthesize the metal-carbon composite in which both the advantages of the high capacity of metal and high conductivity of graphite can be fully utilized. It should also be noted that the chemistry of GICs is very rich.[8] In addition to Bi@Graphite, this method can be further applied to the preparation of Metal@Graphite by using the IVA and VA metals such as Sn, Sb with higher capacities. The Metal@Graphite with metal nanoparticles intercalated in the graphite layers could open up a novel avenue for both the fundamental research and practical application of highly stable, high-rate, alloying-type anode materials for SIBs.

Acknowledgements

This work was supported by the Nanostructures for Electrical Energy Storage (NEES), an Energy Frontier Research Center funded by the US Department of Energy, Office of Science, Basic Energy Sciences, under Award number DESC0001160. The authors gratefully acknowledge the support of the Maryland NanoCenter and its NispLab.

Notes

[1]*Department of Chemical and Biomolecular Engineering, University of Maryland, College Park, MD 20742, USA. E-mail: cswang@umd.edu*
[2]*Department of Chemistry and Biochemistry, University of Maryland, College Park, MD 20742, USA.*

Electronic Supplementary Information (ESI) available: [details of any supplementary information available should be included here]. See DOI: 10.1039/b000000x/

† These authors contribute equally to this work. The authors declare no competing financial interest.

References

1. H. L. Pan, Y. S. Hu and L. Q. Chen, *Energy Environ. Sci.*, 2013, **6**, 2338-2360.
2. H. Kim, H. Kim, Z. Ding, M. H. Lee, K. Lim, G. Yoon and K. Kang, *Adv. Energy Mater.*, 2016, **6**, 1600943.
3. K. Saravanan, C. W. Mason, A. Rudola, K. H. Wong and P. Balaya, *Adv. Energy Mater.*, 2013, **3**, 444-450.
4. C. B. Zhu, K. P. Song, P. A. van Aken, J. Maier and Y. Yu, *Nano Letters*, 2014, **14**, 2175-2180.
5. M. H. Han, E. Gonzalo, N. Sharma, J. M. L. del Amo, M. Armand, M. Avdeev, J. J. S. Garitaonandia and T. Rojo, *Chem. Mater.*, 2016, **28**, 106-116.
6. N. Bucher, S. Hartung, J. B. Franklin, A. M. Wise, L. Y. Lim, H. Y. Chen, J. N. Weker, M. F. Toney and M. Srinivasan, *Chem. Mater.*, 2016, **28**, 2041-2051.
7. C. Y. Yu, J. S. Park, H. G. Jung, K. Y. Chung, D. Aurbach, Y. K. Sun and S. T. Myung, *Energy Environ. Sci.*, 2015, **8**, 2019-2026.
8. M. Dresselhaus and G. Dresselhaus, *Adv. Phys.*, 1981, **30**, 139-326.
9. B. Jache and P. Adelhelm, *Angew. Chem. Int. Edit.*, 2014, **53**, 10169-10173.
10. H. Kim, J. Hong, Y. U. Park, J. Kim, I. Hwang and K. Kang, *Adv. Funct. Mater.*, 2015, **25**, 534-541.
11. Z. F. Li, L. Ma, T. W. Surta, C. Bommierit, Z. L. Jian, Z. Y. Xing, W. F. Stickle, M. Dolgos, K. Amine, J. Lu, T. P. Wu and X. L. Ji, *ACS Energy Letters*, 2016, **1**, 395-401.
12. E. Irisarri, A. Ponrouch and M. R. Palacin, *J. Electrochem. Soc.*, 2015, **162**, A2476-A2482.
13. M. Lao, Y. Zhang, W. Luo, Q. Yan, W. Sun and S. X. Dou, *Adv. Mater.*, 2017, 1700622.
14. M.-S. Balogun, Y. Luo, W. Qiu, P. Liu and Y. Tong, *Carbon*, 2016, **98**, 162-178.
15. R. Raccichini, A. Varzi, S. Passerini and B. Scrosati, *Nat. Mater.*, 2015, **14**, 271.
16. H. Bai, C. Li and G. Shi, *Adv. Mater.*, 2011, **23**, 1089-1115.
17. J. Chen, B. Yao, C. Li and G. Shi, *Carbon*, 2013, **64**, 225-229.
18. P. Lagrange and A. Bendriss-Rerhrhaye, *Carbon*, 1988, **26**, 283-289.
19. M. Rabinovitz, H. Selig and J. Levy, *Angew. Chem. Int. Edit.*, 1983, **22**, 53-53.
20. D. Balzar, N. Audebrand, M. Daymond, A. Fitch, A. Hewat, J. Langford, A. Le Bail, D. Louër, O. Masson and C. N. McCowan, *J. Appl. Crystallogr.*, 2004, **37**, 911-924.
21. R. W. Cheary and A. Coelho, *J. Appl. Crystallogr.*, 1992, **25**, 109-121.
22. X. Zhou, A. C. Soldat and C. Lind, *RSC Adv.*, 2014, **4**, 717-726.
23. A. C. Ferrari, *Solid State Commun.*, 2007, **143**, 47-57.
24. A. C. Ferrari, J. C. Meyer, V. Scardaci, C. Casiraghi, M. Lazzeri, F. Mauri, S. Piscanec, D. Jiang, K. S. Novoselov, S. Roth and A. K. Geim, *Phys. Rev. Lett.*, 2006, **97**, 187401.
25. L. G. Cancado, A. Jorio, E. H. M. Ferreira, F. Stavale, C. A. Achete, R. B. Capaz, M. V. O. Moutinho, A. Lombardo, T. S. Kulmala and A. C. Ferrari, *Nano Letters*, 2011, **11**, 3190-3196.
26. M. M. Lucchese, F. Stavale, E. H. M. Ferreira, C. Vilani, M. V. O. Moutinho, R. B. Capaz, C. A. Achete and A. Jorio, *Carbon*, 2010, **48**, 1592-1597.
27. J. Chen, Y. Zhang, M. Zhang, B. Yao, Y. Li, L. Huang, C. Li and G. Shi, *Chem. Sci.*, 2016, **7**, 1874-1881.
28. R. Raccichini, A. Varzi, D. Wei and S. Passerini, *Adv. Mater.*, 2017, **29**, 1603421.

29. C. Wang, L. Wang, F. Li, F. Cheng and J. Chen, *Adv. Mater.*, 2017, **29**, 1702212.
30. Y. Wen, K. He, Y. Zhu, F. Han, Y. Xu, I. Matsuda, Y. Ishii, J. Cumings and C. Wang, *Nat Commun.*, 2014, **5**, 4033.
31. W. Li, S. L. Chou, J. Z. Wang, J. H. Kim, H. K. Liu and S. X. Dou, *Adv. Mater.*, 2014, **26**, 4037-4042.
32. J. Qian, Y. Chen, L. Wu, Y. Cao, X. Ai and H. Yang, *Chem. Commun.*, 2012, **48**, 7070-7072.
33. Q. Zhang, Y. Wei, H. Yang, D. Su, Y. Ma, H. Li and T. Zhai, *ACS Appl. Mater. Interfaces*, 2017, **9**, 7009-7016.
34. K. Tang, L. Fu, R. J. White, L. Yu, M. M. Titirici, M. Antonietti and J. Maier, *Adv. Energy Mater.*, 2012, **2**, 873-877.
35. S. Zhu, Q. Li, Q. Wei, R. Sun, X. Liu, Q. An and L. Mai, *ACS Appl. Mater. Interfaces*, 2016, **9**, 311-316.
36. S. Li, J. Qiu, C. Lai, M. Ling, H. Zhao and S. Zhang, *Nano Energy*, 2015, **12**, 224-230.
37. M. He, K. Kravchyk, M. Walter and M. V. Kovalenko, *Nano letters*, 2014, **14**, 1255-1262.
38. B. Qu, C. Ma, G. Ji, C. Xu, J. Xu, Y. S. Meng, T. Wang and J. Y. Lee, *Adv. Mater.*, 2014, **26**, 3854-3859.
39. M. Armand and J.-M. Tarascon, *Nature*, 2008, **451**, 652-657.
40. K. Xu, A. von Cresce and U. Lee, *Langmuir.*, 2010, **26**, 11538-11543.
41. X. Dong, L. Chen, J. Liu, S. Haller, Y. Wang and Y. Xia, *Sci. Adv.*, 2016, **2**, e1501038.

Bi@Graphite was synthesized as an ultra-fast and ultra-stable anode material for SIBs with 70% capacity retention at 300C with respect to 1C.